Available online at www.sciencedirect.com
ScienceDirect
Trans. Nonferrous Met. Soc. China 28(2018) 629−641
Transactions of Nonferrous Metals Society of China
www.tnmsc.cn

Deformation behavior and processing maps of Mg−Zn−Y alloy containing *I* phase at elevated temperatures

M. CHAMAN-ARA[1], G. R. EBRAHIMI[1], H. R. EZATPOUR[2]

1. Department of Materials and Polymer Engineering, Hakim Sabzevari University, Sabzevar, Iran;
2. Faculty of Engineering, Sabzevar University of New Technology, Sabzevar, Iran

Received 25 February 2017; accepted 25 June 2017

Abstract: The microstructure and mechanical properties of extruded Mg−Zn alloy containing Y element were investigated in temperature range of 300−450 °C and strain rate range of 0.001−1 s^{-1} through hot compression tests. Processing maps were used to indicate optimum conditions and instability zones for hot deformation of alloys. For Mg−Zn and Mg−Zn−Y alloys, peak stress, temperature and strain rate were related by hyperbolic sine function, and activation energies were obtained to be 177 and 236 kJ/mol, respectively. Flow curves showed that the addition of Y element led to increase in peak stress and decrease in peak strain, and indicated that DRX started at lower strains in Mg−Zn−Y alloy than in Mg−Zn alloy. The stability domains of Mg−Zn−Y alloy were indicated in two domains as 1) 300 °C, 0.001 s^{-1}; 350 °C, 0.01−0.1 s^{-1} and 400 °C, 0.01 s^{-1} and 2) 450 °C, 0.01−0.1 s^{-1}. Microstructural observations showed that DRX was the main restoration mechanism for alloys, and fully dynamic recrystallization of Mg−Zn−Y alloy was observed at 450 °C. The instability domain in Mg−Zn−Y alloy was located significantly at high strain rates. In addition, the instability zone width of Mg−Zn and Mg−Zn−Y alloys increased with increasing strain, and cracks, twins and severe deformation were considered in these regions.

Key words: Mg−Zn−Y alloy; *I* phase; processing map; microstructure; mechanical properties

1 Introduction

Magnesium alloys have several advantages such as light weight, high specific strength, large corrosion resistance, good castability and low cost production which are proper candidates for application in automotive and aerospace industries especially in light-weight structural parts. However, poor formability of these metals due to hexagonal close pack structure (HCP) and activating basal slip system compared to non-basal slip systems leads to limited workability at room temperature [1,2]. Uniform deformation requires five independent slip systems in magnesium alloys while only two slip systems are activated at room temperature. One method to overcome this limitation is reduction of *c*/*a* ratio by alloying, which decreases critical shear stress (CRSS) for activating slip systems [3,4]. It has been known that the addition of rare earth elements such as cerium, calcium, yttrium and strontium, as solutes into the magnesium alloys provides grain refining, improving mechanical properties at room temperature and enhancing the casting characteristics. Among rare earth elements, Y is the most interesting element since it improves both strength and corrosion resistance in Mg alloys [5−8]. According to the thermodynamic calculation and experimental observations of Mg−Zn−Y alloys, several intermetallic phases are found to form by various percentages of Y as *W* phase ($Mg_3Zn_3Y_2$), *I* phase (Mg_3Zn_6Y) and LPSO phase ($Mg_{12}ZnY$) [9−11]. The amounts of Y and Zn/Y ratio in Mg−Zn−Y alloys determine the type of phases formed in microstructure. If this ratio is about 10, Mg_7Zn_3+*α*-Mg phases form. *I*+*α*-Mg phases form as the ratio is in the range of 3−7, the ratio nearly 1.5 leads to the formation of *W* phase and *w*+*z* phases form when the ratio is lower than 1 [10]. Studies have shown that there is a significant interest in *I* phase among the mentioned phases because it causes special properties in Mg−Zn−Y alloy such as significant hardness, high thermal stability, proper corrosion resistance, good abrasion resistance, low *c*/*a* ratio, and grain refining. Increasing the amount of Y element in magnesium alloys causes grain refinement and improves both strength and ductility due to a large number of *I*

Corresponding author: H. R. EZATPOUR; Tel/Fax: +98-5144200750; E-mail: H.R.Ezatpour@gmail.com
DOI: 10.1016/S1003-6326(18)64695-3

phase particles into the matrix which have low surface energy and strong matrix-bonding and develop fine grain microstructure [11−13]. Yield strengths of Mg alloy can be improved from 150 to 450 MPa at room temperature by adding the deferent volume fractions of the *I*-phase [14]. QI et al [9] reported that the yield and ultimate tensile strengths of Mg−Zn−Mn−Y alloy are improved to be 345 and 389 MPa, respectively, with a minor degradation of ductility. ZHANG et al [15] present development of fine-grain microstructure in Mg alloys containing Y after hot deformation process while DRXed fine grains with the size of 2−3 μm form after extrusion process. This is explained that the dispersed particles in these alloys pin grain boundaries and restrict the growth of DRXed grains. TONG et al [16] investigated DRX and texture evolution of Mg−Y−Zn alloy during hot deformation process and observed accelerated DRX through deformed regions containing the particles. BAE et al [17] showed that in deformed alloy with 7.0% Y, *I* phase particles locate at grain boundaries which provide accumulation of dislocations around the grain boundaries during deformation and accelerate the recrystallization process. KWAK et al [18] depicted that the development of new grains can be observed in the adjacent *I* phase during deformation process and a better hot workability is obtained at high strain rate (10 s^{-1}) with a fully recrystallized microstructure and covered by fine grains. Also, XIA et al [19] indicated that fine structure of extruded Mg−Zn−Y−Zr alloy and the basal texture formed after extrusion process promote high workability in different conditions. It is reported that the optimal deformation temperatures and strain rates for Mg−Zn−Y−Zr alloy are 350−400 °C and 0.001−0.1 s^{-1}, respectively. Therefore, the present work is to investigate the effect of the icosahedral phase on microstructure and mechanical properties of Mg−Zn−Y alloy during hot deformation at various temperatures and strain rates. Hot compression tests were carried out in temperature range of 300−450 °C and strain rate range of 0.001−1 s^{-1}. Mechanical data and microstructures results were used to indicate the effect of adding Y element on hot workability of Mg−Zn alloy.

2 Experimental

In the present work, pure magnesium and Mg−7%Y as master alloy were used to product Mg−Zn−Y alloy. Melting and alloying processes were performed in electric resistance furnace using the steel crucible. In order to prevent the oxidation of the melt, the protective CO_2 gas was employed. Then, the melt was cast in the pretreated cylindrical die at 400 °C. The final chemical composition of Mg−Zn and Mg−Zn−Y alloys was characterized by ICP analysis according to the ASTM−E1613 standard to be Mg−5.5Zn and Mg−5.5Zn−1.1Y (mass fraction, %), respectively.

Homogenizing heat treatment was carried out at 450 °C for 16 h and then the sample was quenched in water in order to homogenize the microstructure and solve the precipitations. In the next step, alloys were extruded at 450 °C. Graphite powder was used as lubricant in extrusion process. After extrusion, homogenizing heat treatment was performed in single step cycle at 450 °C for 3 h to remove pre-deformation effects, to complete dynamic recrystallization and to dissolve precipitations formed during process.

In order to investigate warm deformation behavior of the alloys, hot compression tests were carried out in temperature range of 300−450 °C and strain rates of 0.001, 0.01, 0.1 and 1 s^{-1} using Zwick/Roll instrument equipped with an electric furnace with the accuracy of ±5 °C. The samples were covered by Teflon tape as a lubricant to minimize friction effect between sample and die and prevent oxidation. To homogenize samples temperature, they were held at the test temperature for 5 min. At the end of tests, the samples were quenched in water to preserve the microstructure.

Microstructural analyses were performed on the surfaces perpendicular to extrusion axis by optical microscopy (Olympus−GX51). X-ray diffraction analysis was used (Bruker D8 advanced) to indicate phases in the as-cast alloy, using Cu radiation (λ=1.5404 Å). Samples were cut into two pieces and ground up to the grit of $1200^{\#}$ and mechanically polished by 0.03 μm alumina and etched using 10% Nital solution (for as-cast samples) and acetic picral solution (for deformed samples).

3 Results and discussion

3.1 Microstructures after homogenization treatment

Microstructures of homogenized Mg−Zn and Mg−Zn−Y alloys at 450 °C for 16 h are shown in Fig. 1. In Mg−Zn alloy, the equiaxed grains and some Mg_2Zn precipitates are observed in microstructure. Also in some grains, some twins are seen due to annealing treatment (annealing twins) (Fig. 1(a)). In Mg−Zn−Y alloy, after annealing treatment, high volume fraction of *I* phase is clear in grain boundaries. XRD pattern in Fig. 2 indicates the existence of *I* phase in Mg−Zn−Y alloy. XU et al [20] reported that this phase has strong bonding and low interface energy with matrix alloy.

3.2 As-extruded microstructure

Microstructures of Mg−Zn and Mg−Zn−Y alloys after extrusion process are illustrated in Fig. 3. As shown

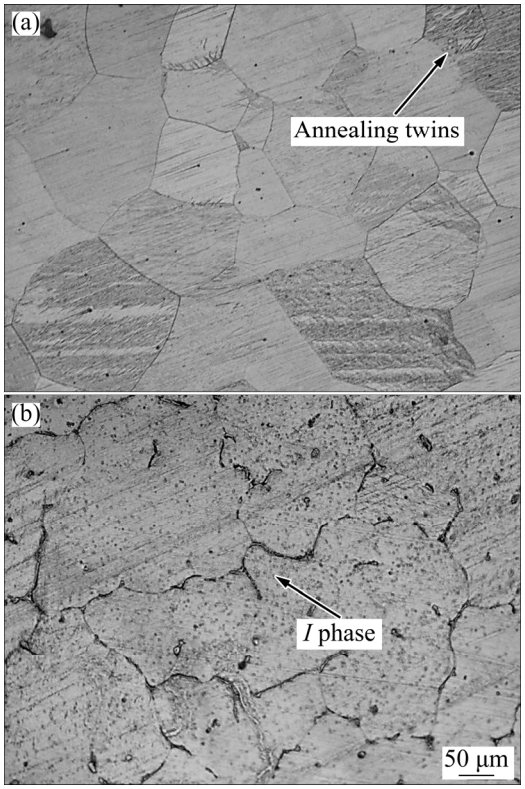

Fig. 1 Microstructures of samples after homogenization treatment at 450 °C for 16 h: (a) Mg−Zn; (b) Mg−Zn−Y

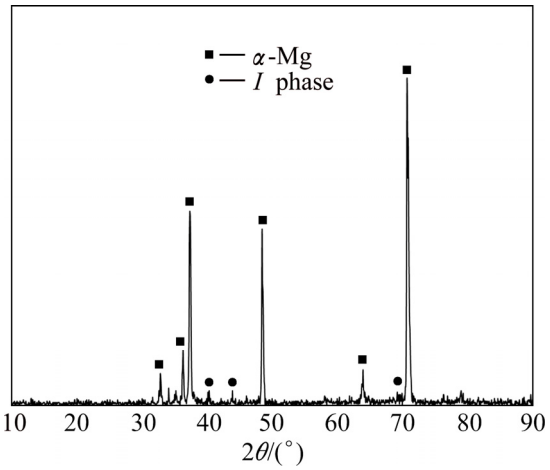

Fig. 2 XRD pattern of as-cast Mg−Zn−Y alloy

in Fig. 3(a), severe twins and inclusions are observed in grains and extruded Mg−Zn−Y alloy (Fig. 3(b)) presents both coarse deformed grains and fine recrystallized grains while *I* phase particles are broken and decorated in extrusion direction. Bimodal microstructure including large and small grains can be due to the presence of *I* phase in Mg−Zn−Y alloy. Recrystallization mechanism induced by high density of dislocations around the particles and pinning phenomenon by *I* phase particles provide bimodal microstructure after extrusion process [20−22].

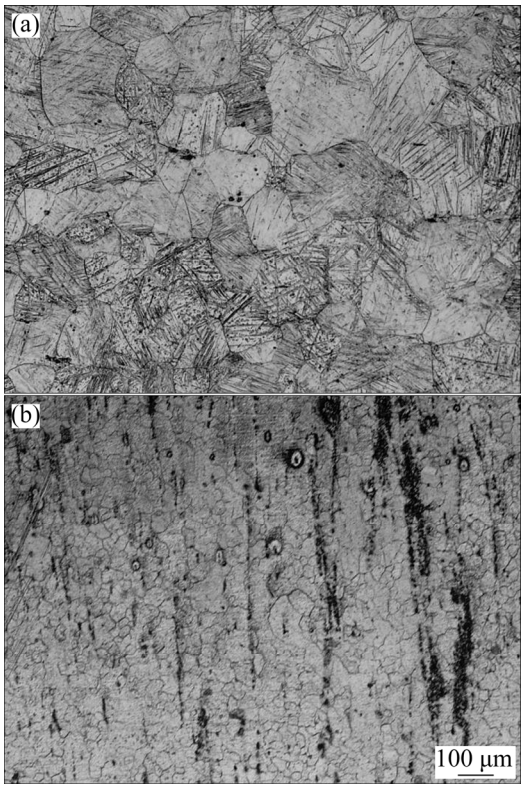

Fig. 3 Microstructures of extruded samples at 450 °C: (a) Mg−Zn; (b) Mg−Zn−Y

3.3 Hot deformation behavior

3.3.1 Stress−strain curves

The hot deformation behaviors of Mg−Zn and Mg−Zn−Y alloys in temperature range of 300−450 °C and strain rates of 0.001, 0.01, 0.1 and 1 s^{-1} (Figs. 4 and 5) show that at high temperatures or low strain rates, evaluations of all true stress – true strain curves are the same, while with increasing strain, firstly, the flow stress rises to a peak stress (σ_p), and then decreases to approach a steady state condition (σ_{ss}). At the first step, two mechanisms, the work hardening and recovery, are simultaneously activated, and the former mechanism is dominant so that flow stress increases continuously to a maximum value. With increasing strain, flow stress drops by activating softening mechanisms particularly dynamic recrystallization (DRX). At the end of process, the stress−strain curves reach steady state. Increase in flow stress to maximum stress can be attributed to accumulation of dislocations and occurrence of work hardening, and subsequent decrease in stress by increasing strain is related to work softening phenomenon. In final step, the balance between work hardening and work softening results in attainment of steady state [21,22]. However, at low temperature and high strain rates, the concave shape shown in compression curves at strains lower than peak strain indicates that twinning controls deformation mechanism [23,24].

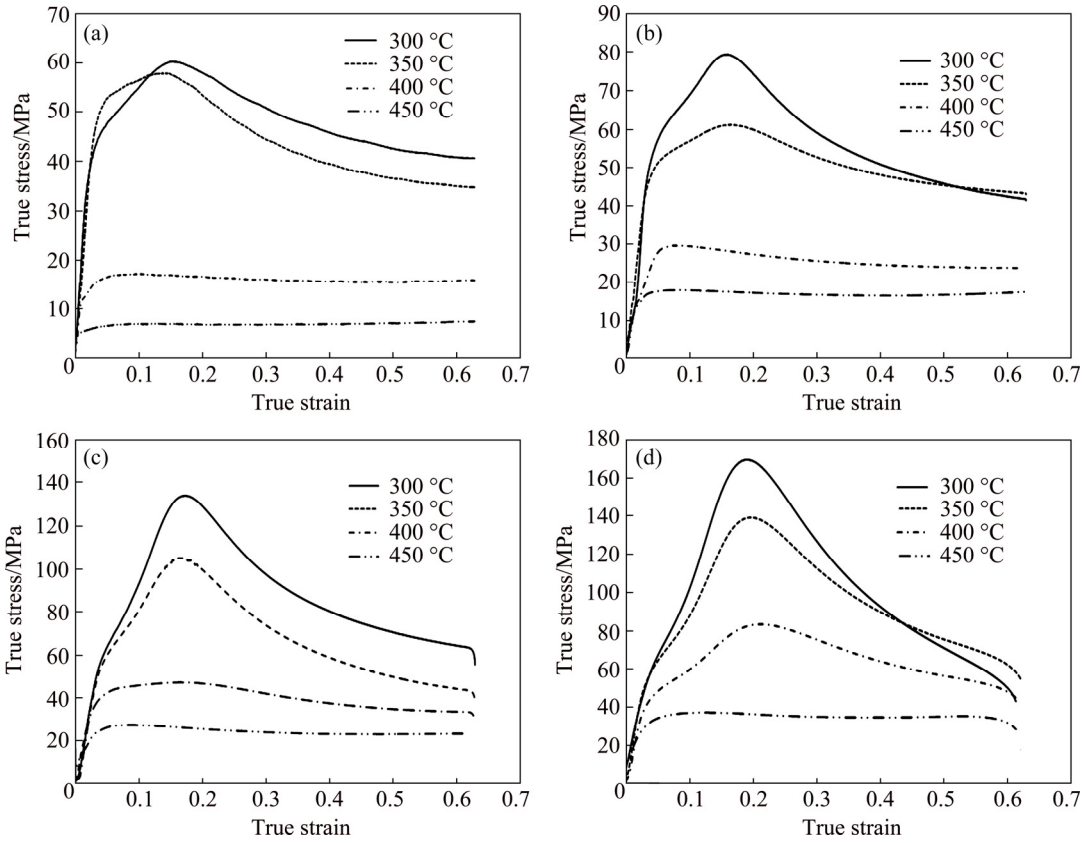

Fig. 4 Hot compression true stress–true strain diagrams of Mg−Zn alloy in temperature range of 300−450 °C and different strain rates: (a) 0.001 s^{-1}; (b) 0.01 s^{-1}; (c) 0.1 s^{-1}; (d) 1 s^{-1}

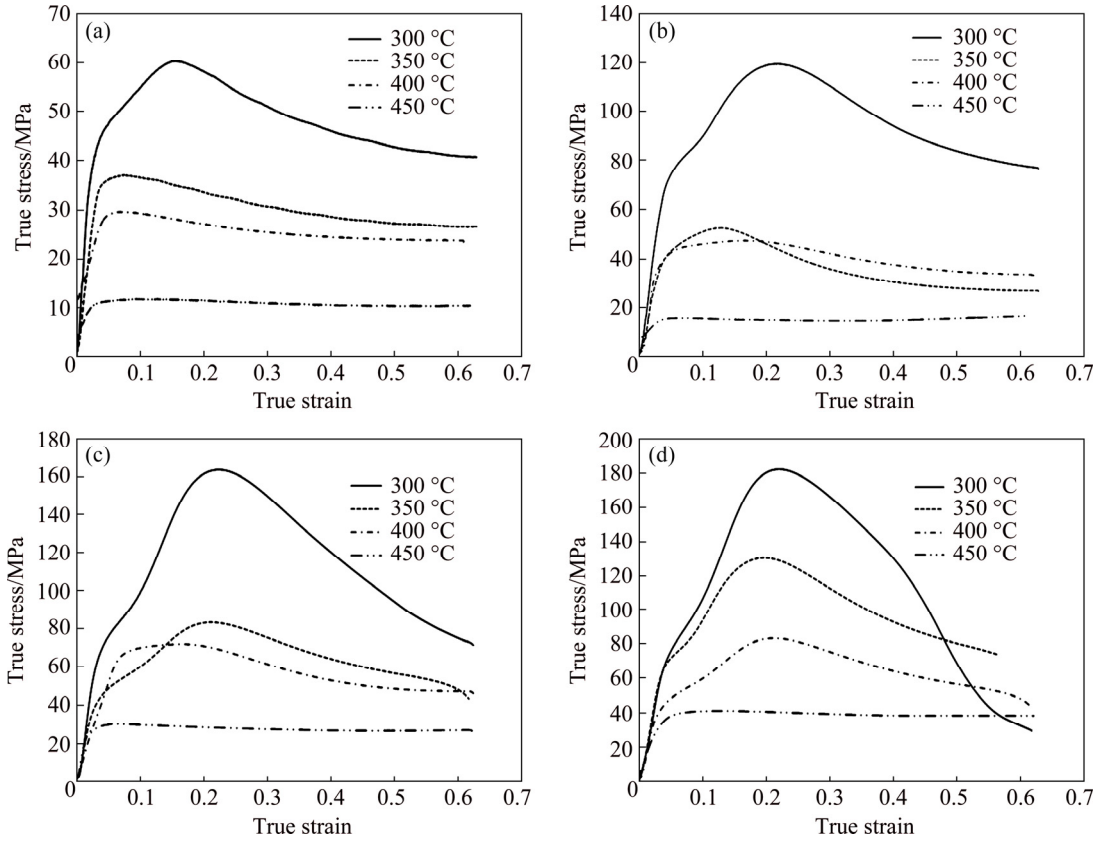

Fig. 5 Hot compression true stress–true strain diagrams of Mg−Zn−Y alloy in temperature range of 300−450 °C and different strain rates: (a) 0.001 s^{-1}; (b) 0.01 s^{-1}; (c) 0.1 s^{-1}; (d) 1 s^{-1}

Figure 6 shows variations of peak stress with temperature at different strain rates. As indicated in Fig. 6, at a definite temperature, the peak stress increases with raising strain rate due to a large number of dislocations and twins formed at high strain rates. Also, it is well known that the flow stress decreases as temperature increases. By increasing temperature at a definite strain rate, the less stress is required for deformation since more slip systems are activated resulting in decrease of the critical resolved shear stress [25]. Besides, higher peak stress of Mg−Zn−Y alloy than Mg−Zn alloy can be due to the presence of *I* particles which provide higher density of dislocations and grain refining.

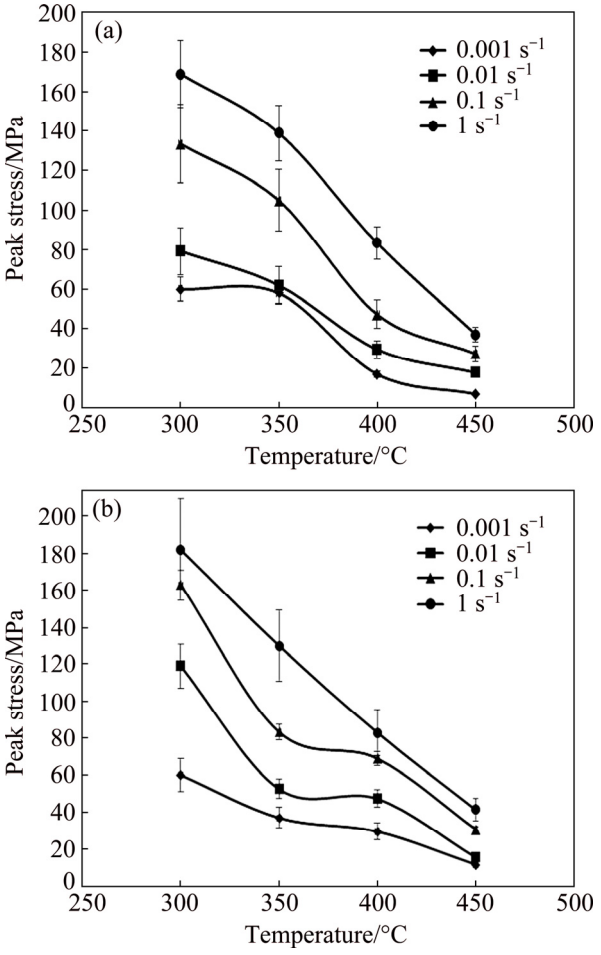

Fig. 6 Variations of peak stress with temperature: (a) Mg−Zn; (b) Mg−Zn−Y

3.3.2 Constitutive equation during hot deformation

The hyperbolic sine function developed by Sellars and Tegart was used in order to determine the relation between hot deformation processing parameters such as flow stress, strain rate and temperature as follows [26]:

$$Z=\dot{\varepsilon}\exp\left(\frac{Q}{RT}\right)=A[\sin(\alpha\sigma)]^n \quad (1)$$

where n, α and A are constants and σ, R, T and Q are peak stress, universal gas constant, deformation temperature and activation energy, respectively. Therefore, activation energy of material can be calculated by taking the natural logarithm of Eq. (1) and interpolating the mechanical testing data obtained from stress−strain curves in Figs. 4 and 5 [27]:

$$Q=2.3R\left.\frac{\partial\log\dot{\varepsilon}}{\partial\lg[\sinh(\alpha\sigma)]}\right|_T\left.\frac{\partial\log[\sinh(\alpha\sigma)]}{\partial(1/T)}\right|_{\dot{\varepsilon}} \quad (2)$$

and,

$$Q=2.3Rns \quad (3)$$

where n is the average slope of $\lg\dot{\varepsilon}$ vs $[\sinh(\alpha\sigma_p)]$ plots and s is the average slope of $\lg[\sinh(\alpha\sigma_p)]$ vs T plots shown in Figs. 7 and 8 for Mg−Zn and Mg−Zn−Y alloys, respectively.

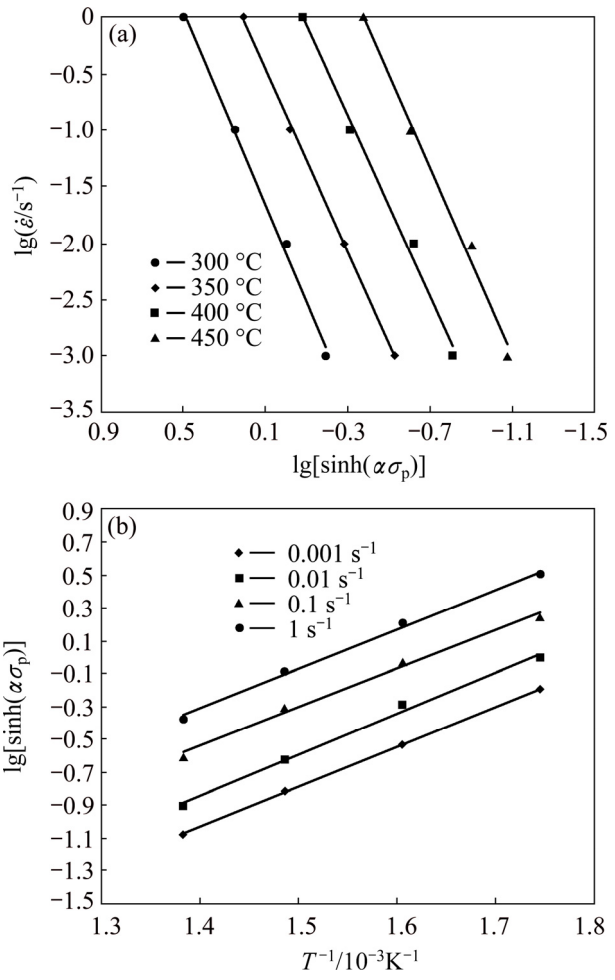

Fig. 7 Logarithmic plots of strain rate vs sinh function of peak stress (a) and sinh function of peak stress vs absolute temperature (b) of Mg−Zn alloy

In Eqs. (1) and (2), α is a variable parameter which is changed to obtain constitutive graphs and it is determined by try and error [28]. All the plots are approximately set in a straight line. Average value of α for Mg−Zn alloy is about 0.009 MPa^{-1} in comparison

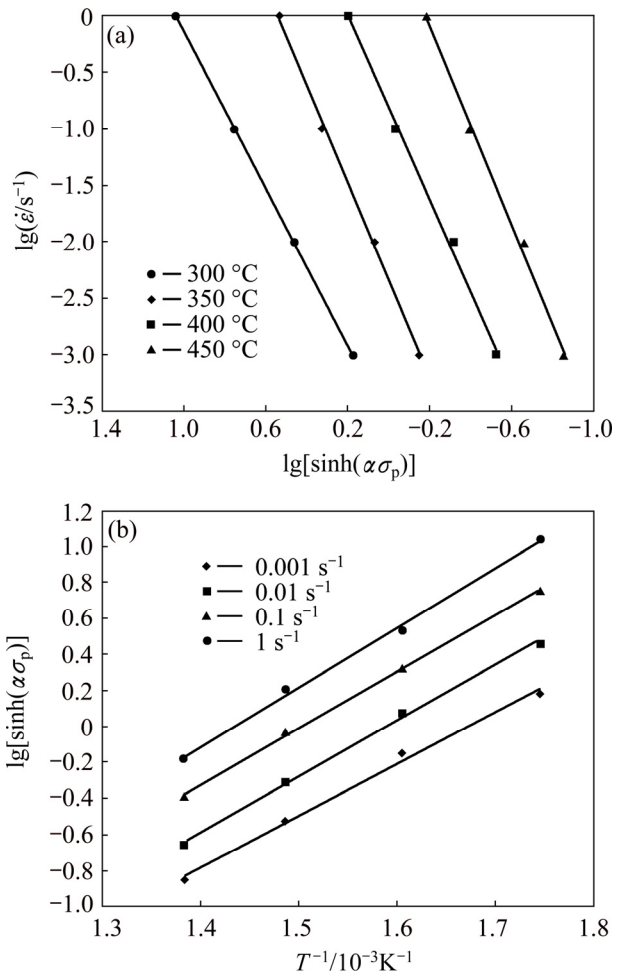

Fig. 8 Logarithmic plots of strain rate vs sinh function of peak stress (a) and sinh function of peak stress vs absolute temperature (b) of Mg−Zn−Y alloy

with 0.015 MPa^{-1} for Mg−Zn−Y alloy. n value for Mg−Zn alloy is calculated to be 3.8, while this value for Mg−Zn−Y alloy is 4.2. Therefore, according to Eq. (3) and average slopes of graphs (Figs. 7 and 8), activation energies for Mg−5.5Zn and Mg−5.5Zn−1.1Y alloys are calculated to be 177 and 236 kJ/mol, respectively, compared with activation energy for pure Mg, 135 kJ/mol [29]. More activation energy of Mg−Zn alloy than pure Mg by about 30% is caused by adding Zn and this value for Mg−Zn−Y alloy is about 75% more than Mg and 27% more than Mg−Zn alloy due to the considerable effect of I phase particles on the hot deformation behavior. It is indicated that the high amount of I phase particles in Mg−Zn−Y alloy provides high density of dislocations during process and limits softening mechanisms at high temperature by decreasing subgrains and grain boundaries motion [18]. The stress−strain curves in Figs. 4 and 5 show that softening mechanism in Mg−Zn−Y alloy starts at higher stresses than Mg−Zn alloy. PRASAD et al [30] reported high activation energy for the cast Mg−3Sn−1Ca alloy (236 kJ/mol) because of the presence of CaMgSn intermetallic particles in the matrix which restrict dislocations motion. XIA et al [19] reported that in Mg alloy containing 5.75Zn, 0.73Y, 0.36Zr (mass fraction, %) (extruded at 400 °C with extrusion ratio of 4), the W phase acts as effective barriers and induces a high Q value in process. Also, high Q value is reported for Mg−9.5Zn−2Y alloy (176.3 kJ/mol) due to the presence of intermetallic compounds in matrix [18].

Figure 9 shows the dependence of logarithm Zener−Holloman parameter to logarithm sinh peak stress which indicates the good fit of the hyperbolic sine function with the correlation coefficient values for the linear regression (R^2), 0.996 and 0.99, for Mg−Zn and Mg−Zn−Y alloys, respectively [31,32]. Therefore, the following constitutive equations can be drawn by plots:

$$Z=1.08\times10^{18}\sinh^{3.8}(0.009\sigma_p) \text{ (Mg−Zn alloy)} \quad (4)$$

$$Z=2.24\times10^{27}\sinh^{4.2}(0.015\sigma_p) \text{ (Mg−Zn−Y alloy)} \quad (5)$$

The dependences of peak stress and peak strain on Zener−Holloman parameter of Mg−Zn and Mg−Zn−Y alloys are shown in Fig. 10. The relation between ε_p and

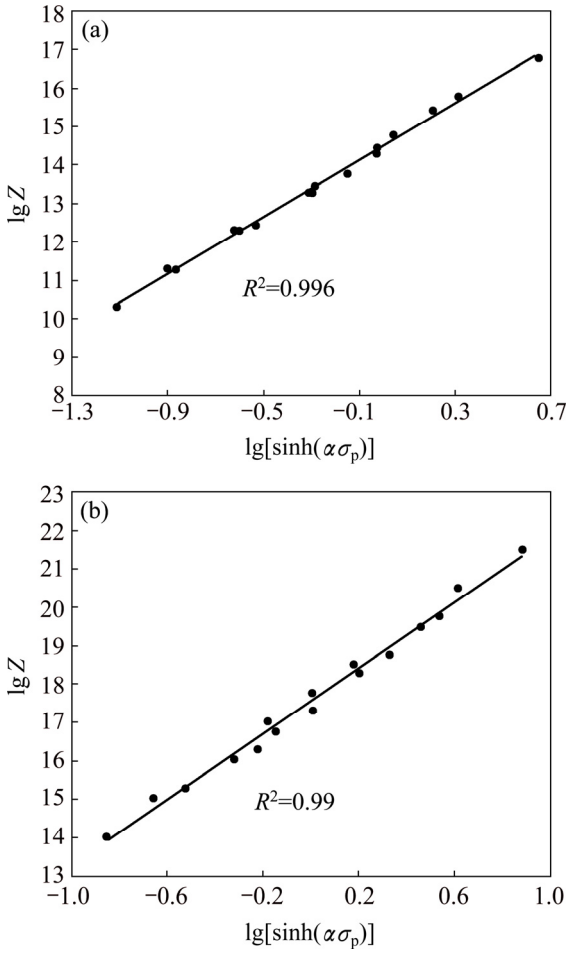

Fig. 9 Variations of logarithm Z vs logarithm sinh peak stress: (a) Mg−Zn; (b) Mg−Zn−Y

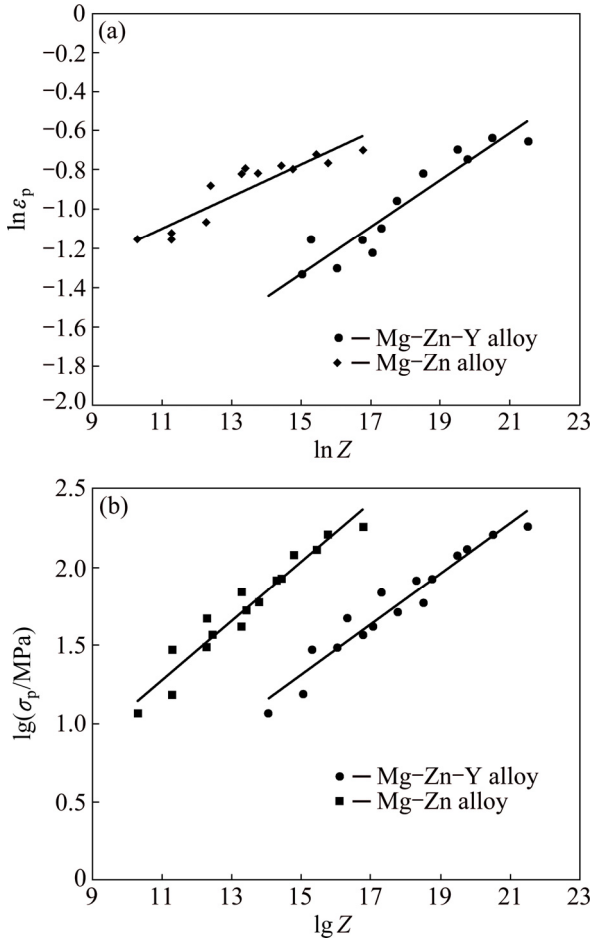

Fig. 10 Logarithmic plots of peak strain (a) and peak stress (b) vs Zener−Holloman parameter of Mg−Zn and Mg−Zn−Y alloys

σ_p with Z parameter are approximately linear and are present in following equations:

$$\lg \varepsilon_p=0.0821\lg Z-2.0053 \text{ (Mg−Zn alloy)} \quad (6)$$

$$\lg \sigma_p=0.1872\lg Z-0.7722 \text{ (Mg−Zn alloy)} \quad (7)$$

$$\lg \varepsilon_p=0.1184\lg Z-3.1027 \text{ (Mg−Zn−Y alloy)} \quad (8)$$

$$\lg \sigma_p=0.1602\lg Z-1.0828 \text{ (Mg−Zn−Y alloy)} \quad (9)$$

With increasing Z (decreasing temperature/ increasing strain rate), peak stress and peak strain increase for both alloys. The higher peak stress and lower peak strain values of Mg−Zn−Y alloy are obtained in comparison with Mg−Zn alloy ($\sigma_{p(Mg-Zn-Y)}=1.1\sigma_{p(Mg-Zn)}$; $\varepsilon_{p(Mg-Zn-Y)}=0.85\varepsilon_{p(Mg-Zn)}$). Addition of Y to Mg−Zn alloy results in higher stress by more work hardening. Y atoms as a intermetallic phase in magnesium matrix especially located in the grain boundaries provide high density of dislocations and act as barriers against dislocation movement and grain boundary migration (more stress) [18,19,30]. Besides, this phase provides sufficient stored energy for DRX in vicinity of grain boundaries and causes to start DRX in lower strains.

3.3.3 Processing maps

In this work, processing maps are designed by dynamic materials model (DMM) based on the variations of stability parameter as a function of temperature and strain rate. In this model, the tool as a source of power and the material as a power dissipater provide the total power as follows [29,33−35]:

$$P=\sigma\dot{\varepsilon}=\int_0^{\dot{\varepsilon}}\sigma \mathrm{d}\dot{\varepsilon}+\int_0^{\sigma}\dot{\varepsilon}\mathrm{d}\sigma \quad (10)$$

where σ is the instantaneous stress and describes the response of the material to the applied strain rate ($\dot{\varepsilon}$) in a given strain (ε).

The first integral (G content) indicates the power dissipated in the form of heat and the second one (J co-content) presents the power dissipated by metallurgical processes such as recovery and dynamic recrystallization (stability domains) and material damage (instability domains) such as formation of Luders' bands, adiabatic shear bands (ASB), localized flow, twins, cracks and holes during deformation [35]. The power-dissipation capacity of the material (J) can be evaluated by defining dimensionless parameter of η according to the following equation [35,36]:

$$\eta=\left(\frac{J}{J_{\max}}\right)=\frac{2m}{m+1} \quad (11)$$

The strain rate sensitivity values ($m=\log\sigma/\log\dot{\varepsilon}$) in different temperatures are measured by interpolating the mechanical testing data as shown in Fig. 11. The changes of η versus temperature and strain rate create a processing map. Also, the dimensionless parameter as instability criterion ($\xi(\dot{\varepsilon})$) is defined by the principle of maximum rate of entropy produced during hot deformation process according to Eq. (12) [29]:

$$\xi(\dot{\varepsilon})=\frac{\partial\ln\left[\frac{m}{m+1}\right]}{\partial\ln\dot{\varepsilon}}+m\le 0 \quad (12)$$

Therefore, in the processing map, the regions with negative value of $\xi(\dot{\varepsilon})$ represent flow instability.

Processing maps of the Mg−Zn and Mg−Zn−Y alloys at peak strain and strain of 0.5 (in steady state zone) are shown in Figs. 12 and 13. Processing map of Mg−Zn alloy in strain of 0.5 (Fig. 12) presents tow domains with higher power dissipation efficiency (η_{max}) which are safe zones for hot deformation of Mg−Zn alloy: Domain I: at 30 0°C, 0.01 s^{-1}; 350 °C, 0.1 s^{-1} and 400−450 °C, 0.1 s^{-1} with maximum efficiency of 40%; Domain II: 450 °C, 0.001 s^{-1} and 400−450 °C, 1 s^{-1} with maximum efficiency of 70%. Processing maps in different strains show that efficiency values increase with increasing strain. Furthermore, with increasing strain at low temperature, stability zone width has been restricted

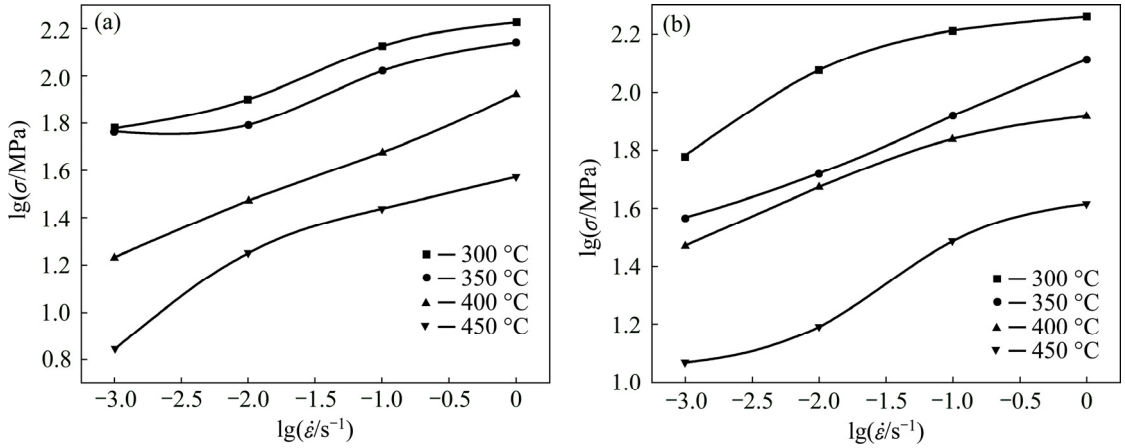

Fig. 11 Logaraitmic plots of stress at strain of 0.5 vs strain rate in temperature range of 300−450 °C: (a) Mg−Zn; (b) Mg− Zn−Y

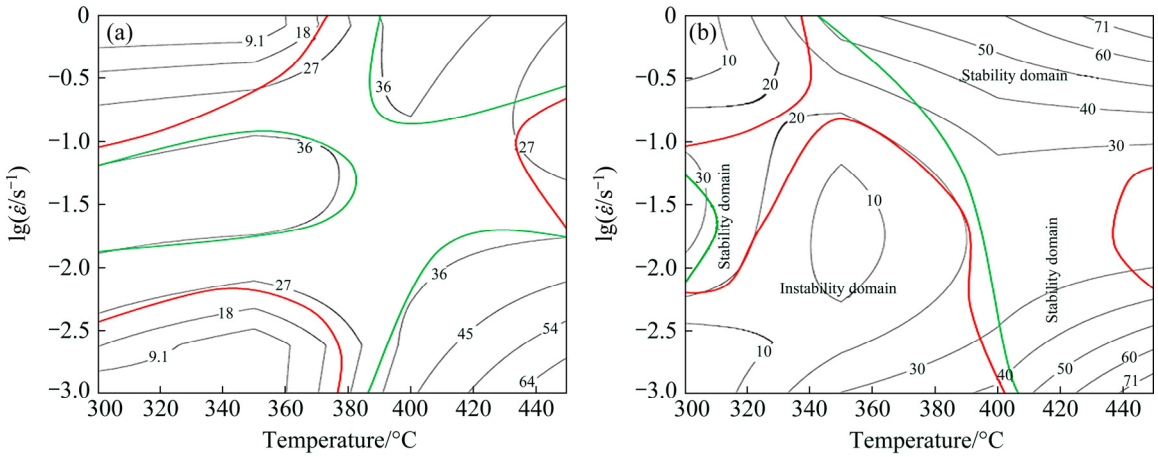

Fig. 12 Processing maps of Mg−Zn alloy: (a) At peak strain; (b) At strain of 0.5

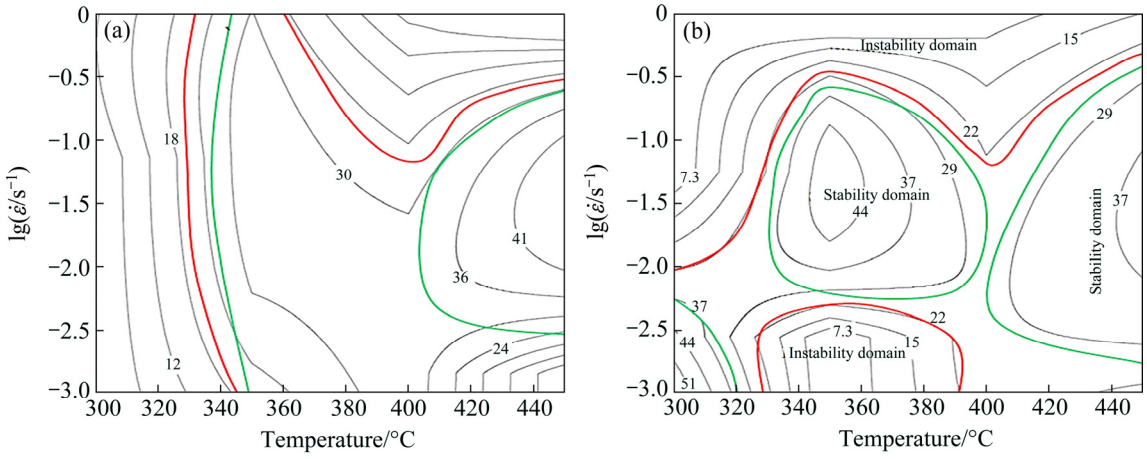

Fig. 13 Processing maps of Mg−Zn−Y alloy: (a) At peak strain; (b) At strain of 0.5

by flow instability, while at high temperature, it has been enlarged. It can be explained that during deformation at low temperature, defects formation can be dominant due to low activated slip systems; while with increasing temperature, activation of more slip systems and facility in dislocations motion and grain boundary migration provide proper conditions for DRX during hot deformation process [15,18].

The processing map of Mg−Zn−Y alloy at strain of 0.5 (Fig. 13) shows that stability deformation occurs at tow domains, including Domain I: 300 °C, 0.001 s^{-1}; 350 °C, 0.01−0.1 s^{-1} and 400 °C, 0.01 s^{-1} with maximum power dissipation efficiency (η_{max}) of 45% and Domain II: 450 °C, 0.01−0.1 s^{-1} with maximum efficiency of 37%. Results show that stability zone width of Mg−Zn−Y alloy is limited by increasing strain and

instability zone has been concentrated at high strain rates in comparison with Mg−Zn alloy. XIA et al [19], reported that instability flow in Mg−Zn−Y−Zr alloy occurs at the higher strain rates due to the stress concentration. Maximum efficiency of Mg−Zn−Y alloy especially at high temperature (400−450 °C) is less than that of Mg−Zn alloy, which can be related to the effect of *I* phase particles on hot deformation behavior of Mg−Zn−Y alloy. At high temperature (e.g. 450 °C, 0.001 s^{-1}), particles act as strong barriers against grain boundaries migration and cause weak workability. Besides, Mg−Zn−Y alloy shows better workability compared with Mg−Zn alloy at lower temperatures. In this case, *I* phase particles provide high density of dislocations and form substructures and subgrains with high angle boundaries and accelerate DRX mechanism, and stress−strain curves indicate that DRX in Mg−Zn−Y alloy starts at lower strains and with larger rate than that in Mg−Zn alloy. Therefore, DRX mechanism in Mg−Zn−Y alloy is considerably dependent on the presence of *I* phase in microstructure [18,19].

3.3.4 Microstructure investigations

Microstructures of Mg−Zn alloy in stability regions and different domains are shown in Figs. 14 and 15. Microstructural observations reveal that at constant strain rate, the grain size and recrystallized volume fraction

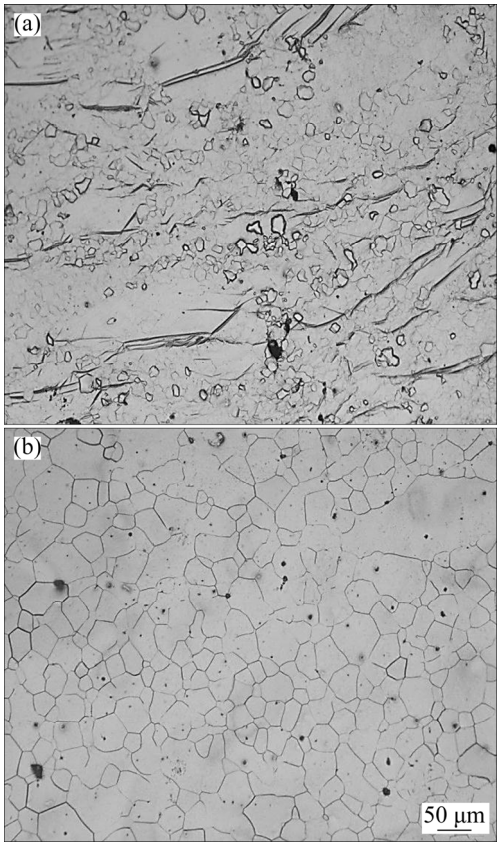

Fig. 14 Optical microstructures of deformed Mg−Zn alloy: (a) 300 °C, 0.01 s^{-1}; (b) 400 °C, 0.01 s^{-1}

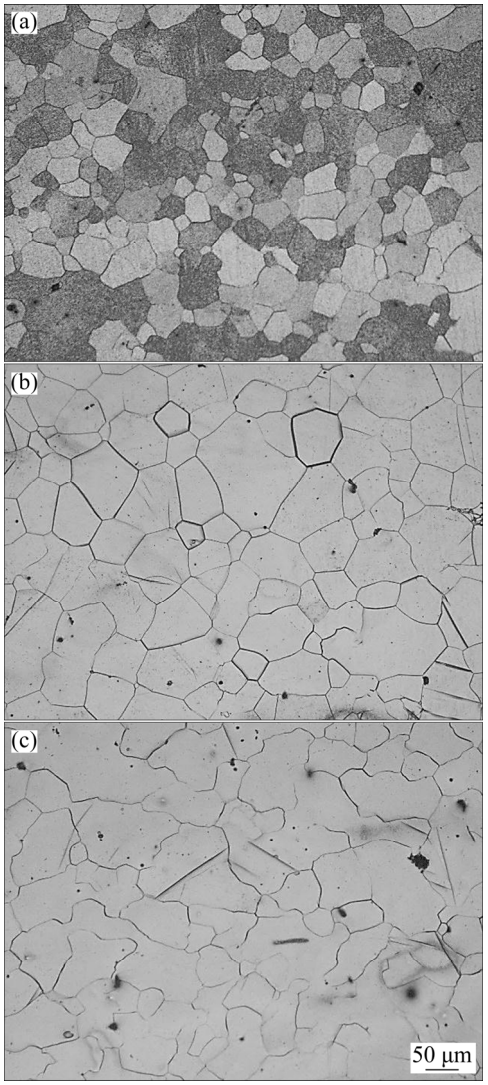

Fig. 15 Optical microstructures of deformed Mg−Zn alloy: (a) 400 °C, 1 s^{-1}; (b) 450 °C, 1 s^{-1}; (c) 450 °C, 0.001 s^{-1}

increase with increment of temperature, while twining content decreases. It should be noted that during deformation at low temperatures, the presence of more twins followed by planes slip rotation provides proper conditions for convenient deformation. At low temperature (e.g. 300 °C, 0.01 s^{-1}), microstructures show bimodal grain size structure containing both deformed grains and recrystallized fine grains and with increasing temperature (400 °C, 0.01 s^{-1}), bimodality in microstructure is decreased by the development of DRX (Figs. 14(a) and (b)) [37]. At high strain rate (1 s^{-1}), fully dynamic recrystallization is observed in temperature range of 400−450 °C, while initial microstructure is covered by the equiaxed grains with high angle boundaries (HAB) (Figs. 15(a)−(c)). Besides, the maximum power dissipation efficiency at 450 °C is remarkably high (η_{max}(450 °C, 0.001 s^{-1})=80%, Fig. 12), which usually predicts the superplastic deformation state. Microstructure result at 450 °C,

0.001 s^{-1} shows coarsening phenomenon of grains by free movement of grain boundaries (Fig. 15(c)), and the presence of some curved and wavy grain boundaries indicates grain boundary sliding at low strain rate. At low temperatures, DRX is controlled by dislocation climbing process and depends on lattice self-diffusion, and at the high temperatures, many slip planes are active and DRX is affected by activating second-order pyramidal slip and cross-slip [38].

Microstructures of Mg−Zn−Y alloy in stability regions are shown in Fig. 16. Generally, DRXed grains in alloy are very smaller than those in Mg−Zn alloy with more volume fraction due to the presence of *I* phase particles, because (1) the stress−strain curves show that in Mg−Zn alloy containing particles, DRX starts at lower strains and with more rate and (2) the particles act as barrier. At low temperatures (Figs. 16(a) and (b)), high volume fraction of very fine DRXed grains are seen in vicinity of grain boundaries. In this zone, during deformation, *I* phase particles develop high volume of dislocations and stored energy due to decrease in the dislocation pile-up, so the concentrated stress is difficult to release by DRX; therefore, nucleation of very fine grains in grain boundaries is observed in this zone [39]. At high temperature (450 °C), size and volume fraction of *I* phase have remarkably decreased and particles are uniformly dispersed into the matrix. Therefore, in this zone, DRXed grain size grows considerably and microstructure is covered by new grains, and a full DRX with the equiaxed grains and smooth grain boundaries (high angle boundaries (HAB)) is obtained at strain rate of 0.1 s^{-1} (Figs. 16(c) and (d)) [38].

Instability zones of Mg−Zn alloy at different strains (ε_p, $\varepsilon_{0.5}$) are shown in Fig. 12. Maps present that instability zone width increases with increasing strain especially at low temperatures, which indicates defects formation with continuation of deformation. Microstructures of these zones show the presence of cracks, twins and flow localization. At low temperature and high strain rates, high volume fraction of twins and cracks are observed in microstructure (Fig. 17(a)), and at low strain rate, flow localization phenomenon and crack develop in instable conditions (Fig. 17(b)) [40−43].

In Mg−Zn−Y alloy, with increasing strain, instability domains have located at high strain rates (Fig. 13). Microstructure analysis of instability domain at 350 °C and 0.001 s^{-1} shows formation of crack in vicinity of *I* phase particles (Fig. 18(a)). At high strain rates, at temperature of 300 °C, sever deformation is mostly dominated, while kinked grain boundaries are considered in microstructure (Fig. 18(b)) [43]. Also, breaking and separating particles, nucleation of crack around the separated particles and more twins are observed in microstructure at higher temperatures (Figs. 18(c) and (d)).

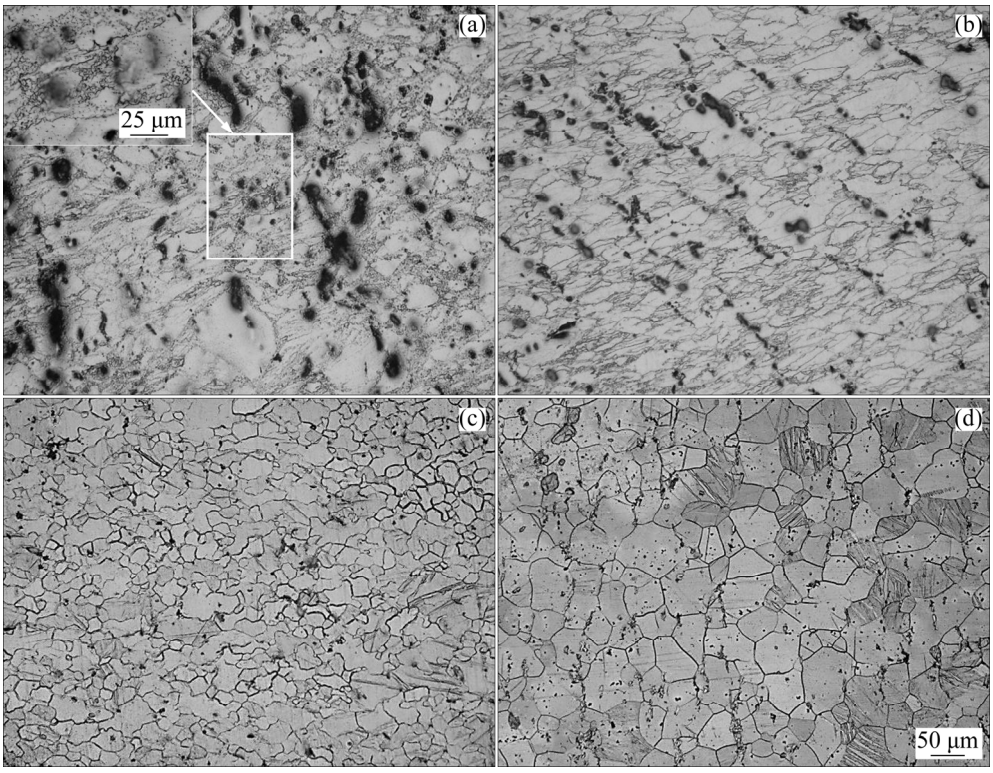

Fig. 16 Optical microstructures of deformed Mg−Zn−Y alloy: (a) 300 °C, 0.001 s^{-1}; (b) 350 °C, 0.01 s^{-1}; (c) 450 °C, 0.01 s^{-1}; (d) 450 °C, 0.1 s^{-1}

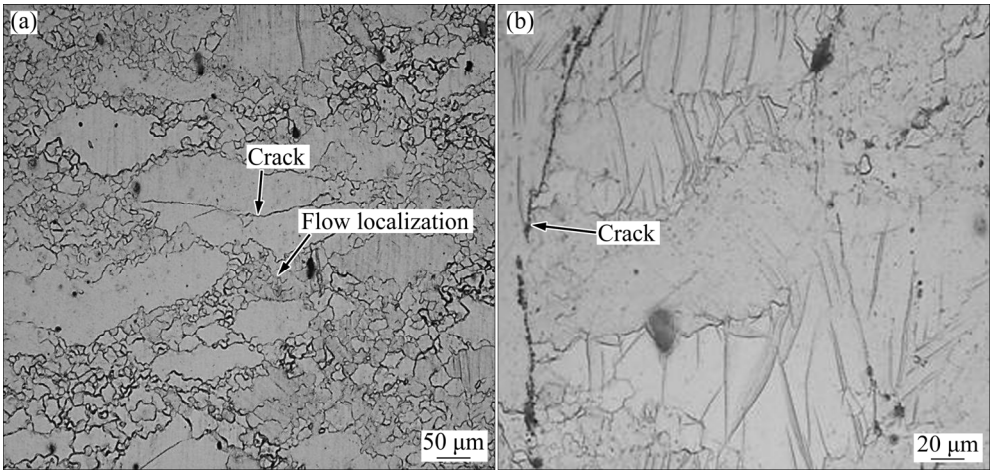

Fig. 17 Optical microstructures of deformed Mg−Zn alloy: (a) 300 °C, 1 s^{-1}; (b) 350 °C, 0.01 s^{-1}

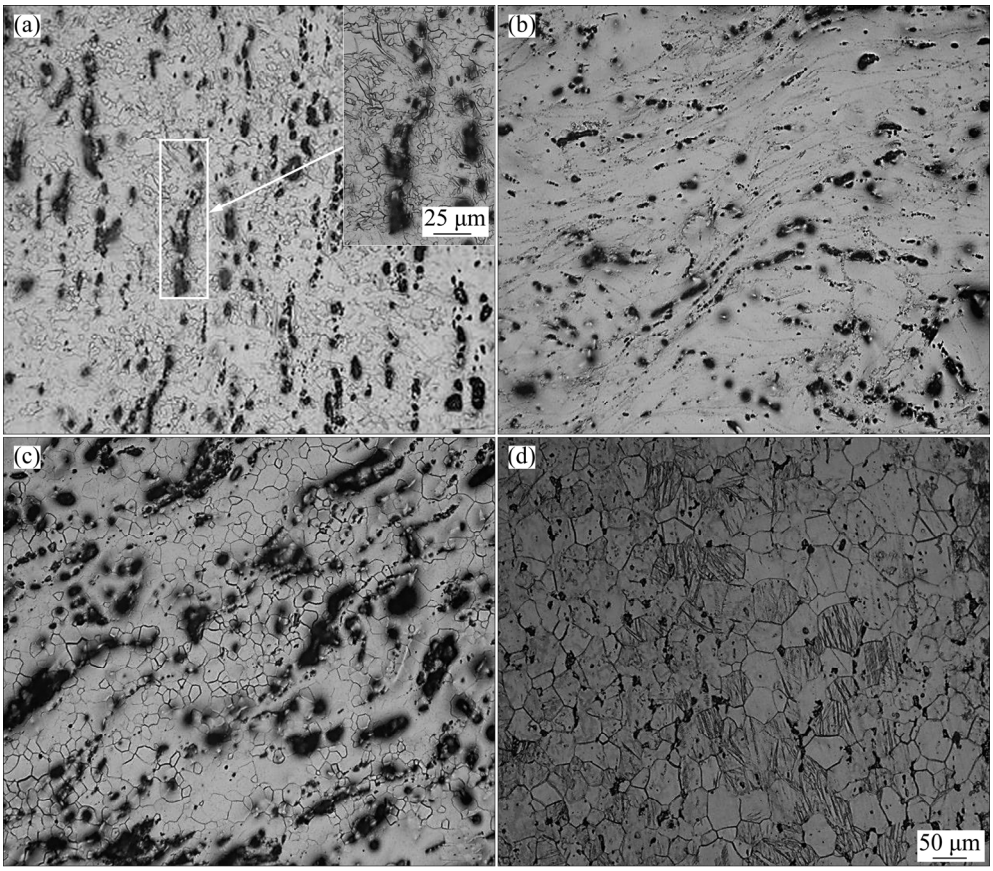

Fig. 18 Optical microstructures of deformed Mg−Zn−Y alloy: (a) 350 °C, 0.001 s^{-1}; (b) 300 °C, 1 s^{-1}; (c) 350 °C, 1 s^{-1}; (d) 450 °C, 1 s^{-1}

4 Conclusions

1) The true stress−true strain curves of Mg−Zn−Y and Mg−Zn alloys indicated that the addition of Y element increases the peak stress and decreases the peak strain.

2) The activation energies of Mg−Zn and Mg−Zn−Y alloys were obtained to be 177 and 236 kJ/mol, respectively.

3) The stability domains for hot deformation of Mg−Zn alloy were allocated at Domain I: 300 °C, 0.01 s^{-1}; 350 °C, 1 s^{-1} and 400−450 °C, 0.1 s^{-1} with maximum efficiency of 40%; Domain II: 450 °C, 0.001 s^{-1} and 400−450 °C, 1 s^{-1} with maximum efficiency of 70%.

4) The stability domains of deformation for Mg−Zn−Y alloy occurred in two domains including Domain I: 300 °C, 0.001 s^{-1}; 350 °C, 0.01−0.1 s^{-1} and 400 °C, 0.01 s^{-1} with maximum efficiency of 45%, and Domain II: 450 °C, 0.01−0.1 s^{-1} with maximum efficiency of 35%.

5) DRX was the main restoration mechanism for materials, and fully dynamic recrystallization for Mg−Zn−Y alloy occurred at temperature of 450 °C.

6) Instability zone width of Mg−Zn and Mg−Zn−Y alloys increased with increasing strain, and cracks, twins and sever deformation were considered in these regions.

References

[1] MORDIKE B, EBERT T. Magnesium: Properties−applications−potential [J]. J Mater Sci Eng A, 2001, 302: 37−45.

[2] TEKUMALLA S, SEETHARAMAN S, ALMAJID A, GUPTA M. Mechanical properties of magnesium-rare earth alloy systems: A review [J]. J Met, 2014, 5: 1−39.

[3] HEHMANN F, SOMMER F, PREDEL B. Extension of solid solubility in magnesium by rapid solidification [J]. Mater Sci Eng A, 1990, 125: 249−265.

[4] REED-HILL R, ROBERTSON W. Additional modes of deformation twinning in magnesium [J]. Acta Met, 1957, 5: 717−727.

[5] CHEN Q, SHU D, ZHAO Z, ZHAO Z, WANG Y, YUAN B. Microstructure development and tensile mechanical properties of Mg−Zn−RE−Zr magnesium alloy [J]. Mater Des, 2012, 40: 488−496.

[6] CHENA Q, LIN J, SHU D, HU C, ZHAO Z, KANG F, HUANG S, YUAN B. Microstructure development, mechanical properties and formability of Mg−Zn−Y−Zr magnesium alloy [J]. Mater Sci Eng A, 2012, 554: 129−141.

[7] ZHAO Z, CHEN Q, YANG L, SHU D, ZHAO Z. Microstructure and mechanical properties of Mg−Zn−Y−Zr alloy prepared by solid state recycling [J]. Transactions of Nonferrous Metals Society of China, 2011, 21: 265−271.

[8] LIN D, WANG L, LIU Y, CUI J, LE Q. Effects of plastic deformation on precipitation behavior and tensile fracture behavior of Mg−Gd−Y−Zr alloy [J]. Transactions of Nonferrous Metals Society of China, 2011, 21: 2160−2167.

[9] QI F G, ZHANG D F, ZHANG X H, PAN F S. Effect of Y addition on microstructure and mechanical properties of Mg−Zn−Mn alloy [J]. Transactions of Nonferrous Metals Society of China, 2014, 24: 1352−1364.

[10] SINGH L K, SRINIVASAN A, PILLAI U, JOSEPH M, PAI B. The effect of yttrium addition on the microstructure and mechanical properties of Mg alloys [J]. Trans Indian Institute Met, 2015, 68: 331−339.

[11] ZENG X, ZHANG Y, LU C, DING W, WANG Y, ZHU Y. Precipitation behavior and mechanical properties of a Mg−Zn−Y−Zr alloy processed by thermo-mechanical treatment [J]. J Alloys Compd, 2005, 395: 213−219.

[12] XU D K, LIU L, XU Y B, HAN E H. Effect of microstructure and texture on the mechanical properties of the as-extruded Mg−Zn−Y−Zr alloys [J]. Mater Sci Eng A, 2007, 443: 248−256.

[13] ZHANG Z, LIU X, HU W, LI J, LE Q, BAO L, ZHU Z, CU J. Microstructures, mechanical properties and corrosion behaviors of Mg−Y−Zn−Zr alloys with specific Y/Zn mole ratios [J]. J Alloys Compd, 2011, 624: 116−125.

[14] XU D K, HAN E H. Effects of icosahedral phase formation on the microstructure and mechanical improvement of Mg alloys: A review, Progress in Natural Science [J]. Mater Int, 2012, 22: 364−385.

[15] ZHANG Y, ZENG X, LIU L, LU C, ZHOU H, LI Q, ZHU Y. Effects of yttrium on microstructure and mechanical properties of hot-extruded Mg−Zn−Y−Zr alloys [J]. J Alloys Compd, 2015, 624: 116−125.

[16] TONG L B, LI X, ZHANG D P, CHENG L R, MENG J, ZHANG H J. Dynamic recrystallization and texture evolution of Mg−Y−Zn alloy during hot extrusion process [J]. Mater Charact, 2014, 92: 77−83.

[17] BAE D H, KIM S H, KIM D H, KIM W T. Deformation behavior of Mg−Zn−Y alloys reinforced by icosahedral quasicrystalline particles [J]. Acta Mater, 2002, 50: 2343−2356.

[18] KWAK T Y, LIM H K, KIM W J. Hot compression characteristics and processing maps of a cast Mg−9.5Zn−2.0Y alloy with icosahedral quasicrystalline phase [J]. J Alloys Compd, 2015, 644: 645−653.

[19] XIA X, CHEN Q, HUANG S, LIN J, HU C, ZHAO Z. Hot deformation behavior of extruded Mg−Zn−Y−Zr alloy [J]. J Alloys Compd, 2015, 215: 308−316.

[20] XU S, ZHENG M, KAMADO S, WU K, WANG G, LV X. Dynamic microstructural changes during hot extrusion and mechanical properties of a Mg−5.0Zn−0.9Y−0.16Zr (wt.%) alloy [J]. Mater Sci Eng A, 2011, 528: 4055−4067.

[21] HAGIHARA K, KINOSHITA A, SUGINO Y, YAMASAKI M, KAWAMURA Y, YASUDA H. Plastic deformation behavior of Mg97Zn1Y2 extruded alloys [J]. Transactions of Nonferrous Metals Society of China, 2010, 20: 1259−1268.

[22] SINGH A, NAKAMURA M, WATANABE M, KATO A, TSAI A. Quasicrystal strengthened Mg−Zn−Y alloys by extrusion [J]. Scripta Mater, 2003, 49: 417−422.

[23] SHANG S J, DENG K K, NIE K B, LI J C, ZHOU S S, XU F J, FAN J F. Microstructure and mechanical properties of SiC_p/Mg−Al−Zn composites containing $Mg_{17}Al_{12}$ phases processed by low-speed extrusion [J]. J Mater Sci Eng A, 2014, 610: 243−249.

[24] WANG J, HIRTH J P, TOMÉ C N. Twinning nucleation mechanisms in hexagonal-close-packed crystals [J]. Acta Mater, 2009, 57: 5521−5530.

[25] RAVI KUMAR N V, BLANDIN J J, DESRAYAUD C, MONTHEILLET F, SUE´RY M. Grain refinement in AZ91 magnesium alloy during thermomechanical processing [J]. Mater Sci Eng A, 2003, 359: 150−157.

[26] SELLARS C M, MCTEGART W J. On the mechanism of hot deformation [J]. Acta Meter, 1966, 14: 1136−1138.

[27] EZATPOUR H R, SAJJADI S A, HADDAD SABZEVAR M, CHAICHI A, EBRAHIMI G R. Processing map and microstructure evaluations of AA6061-Al_2O_3 nanocomposite at different temperatures [J]. Transaction of Nonferrous Metals Society of China, 2017, 27: 1−9.

[28] EZATPOUR H R, SAJJADI S A, HADDAD-SABZEVAR M, EBRAHIMI G R. Hot deformation and processing maps of K310 cold work tool steel [J]. J Mater Sci Eng A, 2012, 550: 152−159.

[29] FROST H J, ASHBY M F. Deformation mechanism maps, the plasticity and creep of metals and ceramics [M]. London: Pergamon Press, 1982.

[30] PRASAD Y V R K, RAO K P, HORT N, KAINER K U. Hot working parameters and mechanisms in as-cast Mg−3Sn−1Ca alloy [J]. Mater Let, 2008, 62: 4207−4209.

[31] EBRAHIMI G R, MALDAR A R, EBRAHIMI R, DAVOODI A. Effect of thermomechanical parameters on dynamically recrystallized grain size of AZ91 magnesium alloy [J]. J Alloys Compd, 2011, 509: 2703−2708.

[32] KHAN A S, PANDEY A, GNÄUPEL-HEROLD T, MISHRA R K. Mechanical response and texture evolution of AZ31 alloy at large strains for different strain rates and temperatures [J]. Int J Plasticity,

2011, 27: 688−706.
[33] RAJ R. Development of a processing map for use in warm-forming and hot-forming processes [J]. Met Trans A, 1981, 12: 1089−1097.
[34] PRASAD Y V R K, SASIDHARA S. Hot working guide: A compendium on processing maps [M]. Metals Park, Ohio: ASM International, 1997.
[35] PRASAD Y V R K. Processing maps: A status report [J]. J Mater Eng Perform, 2003, 12: 638−645.
[36] ZIEGLER H. Progress in solid mechanics [M]. New York: John Wiley & Sons, 1963: 93−193.
[37] BARNETT M R, KESHAVARZ Z, BEER A G, ATWELL D. Influence of grain size on the compressive deformation of wrought Mg−3Al−1Zn [J]. Acta Mater, 2004, 52: 5093−5103.
[38] WU X, LIU Y. Superplasticity of coarse-grained magnesium alloy [J]. Scripta Mater, 2002, 46: 269−274.
[39] CHANGIZIAN P, ZAREI-HANZAKI A, ABEDI H. On the recrystallization behavior of homogenized AZ81 magnesium alloy: The effect of mechanical twins and γ precipitates [J]. Mater Sci Eng A, 2012, 558: 44−51.
[40] EZATPOUR H R, HADDAD SABZEVAR M, SAJJADI S A, HUANG Y Z. Investigation of work softening mechanisms and texture in a hot deformed 6061 aluminum alloy at high temperature [J]. Mater Sci Eng A, 2014: 606: 240−247.
[41] BAI Y, BODD N. Adiabatic shear localization [M]. Oxford: Pergamon Press, 1992.
[42] OWOLABI G M, ODESHI A G, SINGH M N K, BASSIM M N. Dynamic shear band formation in aluminum 6061-T6 and aluminum 6061-T6/Al_2O_3 composites [J]. Mater Sci Eng A, 2007, 457: 114−119.
[43] McQUEEN H J, XIA X, CUI Y, LI B, MENG Q. Solution and precipitation effects on hot workability of 6201 alloy [J]. Mater Sci Eng A, 2001, 319−321: 420−424.

含 *I* 相 Mg−Zn−Y 合金的高温变形行为和加工图

M. CHAMAN-ARA[1], G. R. EBRAHIMI[1], H. R. EZATPOUR[2]

1. Department of Materials and Polymer Engineering, Hakim Sabzevari University, Sabzevar, Iran;
2. Faculty of Engineering, Sabzevar University of New Technology, Sabzevar, Iran

摘　要：通过热压缩试验(温度 300~450 °C，应变速率 0.001~1 s^{-1})研究挤压态含 Y 元素的 Mg−Zn 合金的微观组织和力学性能。用热加工图反映合金热变形的最佳条件和非稳定区。Mg−Zn 和 Mg−Zn−Y 合金的峰值应力、温度和应变速率的关系符合双曲正弦函数，激活能分别为 177 kJ/mol 和 236 kJ/mol。流变应力曲线表明，Y 的添加会增加峰值应力并减小峰值应变，且 Mg−Zn−Y 合金发生动态再结晶所需的应变比 Mg−Zn 合金的小。Mg−Zn−Y 合金的稳定区发生在：1) 300 °C，0.001 s^{-1}；350 °C，0.01−0.1 s^{-1} 和 400 °C，0.01 s^{-1}；2) 450 °C，0.01−0.1 s^{-1}。显微组织的观察结果显示，合金中主要的恢复机制是动态再结晶，Mg−Zn−Y 合金发生完全动态再结晶的温度为 450 °C。在高应变速率下，Mg−Zn−Y 合金明显形成非稳定区。另外，Mg−Zn 和 Mg−Zn−Y 合金的非稳定区域宽度随应变的增加而增加，这些区域还发生了孪生和严重变形。

关键词：Mg−Zn−Y 合金；*I* 相；加工图；微观组织；力学性能

(Edited by Bing YANG)